e-ISSN 2083–4640
ISSN 1507–1367

RESEARCH PAPER

Reports of Practical Oncology and Radiotherapy
2022, Volume 27, Number 5, pages: 768–777
DOI: 10.5603/RPOR.a2022.0086
Submitted: 31.05.2022
Accepted: 05.07.2022

Improved biological dosimetric margin model for different PTV margins with stereotactic body radiation therapy in homogeneous and nonhomogeneous tumor regions

Daisuke Kawahara[1], Akito Saito[1], Yasushi Nagata[1, 2]

[1]Department of Radiation Oncology, Institute of Biomedical & Health Sciences, Hiroshima University, Hiroshima, Japan
[2]Hiroshima High-Precision Radiotherapy Cancer Center, Hiroshima, Japan

ABSTRACT

Background: The purpose of this study was to improve the biological dosimetric margin (BDM) corresponding to different planning target volume (PTV) margins in homogeneous and nonhomogeneous tumor regions using an improved biological conversion factor (BCF) model for stereotactic body radiation therapy (SBRT).

Materials and methods: The PTV margin was 5–20 mm from the clinical target volume. The biologically equivalent dose (BED) was calculated using the linear–quadratic model. The biological parameters were $\alpha/\beta = 10$ Gy, and the dose per fraction (DPF) was d = 3–20 Gy/fr. The isocenter was offset at intervals of 1 mm; 95% of the clinical target volume covered more than 90% of the prescribed physical dose, and BED was defined as biological and physical DMs. The BCF formula was defined as a function of the DPF.

Results: The difference in the BCF caused by the DPF was within 0.05 for the homogeneous and nonhomogeneous phantoms. In the virtual nonhomogeneous phantom, the data with a PTV margin of 10–20 mm were not significantly different; thus, these were combined to fit the BCF. In the virtual homogeneous phantom, the BCF was fitted to each PTV margin.

Conclusions: The current study improved a scheme to estimate the BDM considering the size of the PTV margin and homogeneous and nonhomogeneous regions. This technique is expected to enable BED-based treatment planning using treatment systems based on physical doses for SBRT.

Key words: SBRT; biological equivalent dose; dosimetric margin; photon therapy

Rep Pract Oncol Radiother 2022;27(5):768–777

Introduction

Dose-volume histograms (DVHs) are used to evaluate treatment planning. Dose-volume constraints indicate that organs should not receive doses exceeding certain limits. Radiobiological studies have exhibited the same biological effect by providing a biologically effective dose (BED) through different fractionation schemes or dose per fraction [1–3]. Fowler showed that BED modeling is useful for understanding normal tissue and tumor responses across different fractionation schemes and treatment methods [4].

The relative biological effectiveness depends on the dose level, which is the dose per fraction (DPF) and the number of dose fractions. Our previous

Address for correspondence: Daisuke Kawahara, PhD, Section of Radiation Therapy, Department of Clinical Support, Hiroshima University Hospital, 1-2-3 Kasumi, Minami-ku, Hiroshima, Hiroshima 734–8551, Japan, tel: +81-82-257-1545, fax: +81-82-257-1546; e-mail: daika99@hiroshima-u.ac.jp

study proposed a dosimetric margin (DM) that considers dose perturbation based on the setup uncertainties. Moreover, biological effectiveness was incorporated in the DM and the biological conversion factor (BCF) between the physical DM (PDM), and biological DM (BDM) was proposed. We evaluated the PDM and BDM with regard to lung stereotactic body radiotherapy (SBRT). Our previous study showed that the size of the planning target volume (PTV) margin negligibly affected the BDM and PDM. However, the effect of the PTV margin was not included in this study. Moreover, the dose perturbation is different for different density materials, energies, dose calculation algorithms, and interplay effects. The penumbra width increases for high-energy photon beams [5]. Lateral scattered electrons generated by the beam path increase, and the penumbra width increases when low-density materials are present [6–8]. Dose build-up and rebuild-down effects occur in the peripheral tumor region around the low-density materials. It decreases with the small field size [5]. For the intensity-modulated radiotherapy (IMRT) treatment, the interplay effect occurs at hot or cold dose spots [9, 10]. Consequently, these dose perturbations may affect the BDM distribution and BCF model.

In the current study, we evaluated the PDM and BDM involving dose perturbation, which focused on the setup uncertainty in homogeneous and nonhomogeneous regions. An improved BCF model corresponding to the PTV margin was proposed.

Materials and methods

An anthropomorphic phantom, RANDO (The Phantom Laboratory, Salem, NY), was scanned using computed tomography (CT) (LightSpeed RT16, GE Healthcare, Little Chalfont, UK). The tube voltage was 120 kVp, and the slice interval and thickness were 2.5 mm. The scanned CT images were transferred to the treatment planning system — RayStation ver. 6.0 (RaySearch Medical Laboratories AB, Stockholm, Sweden). In treatment planning, a linear accelerator was used — TrueBeam (Varian Medical Systems, Palo Alta, CA, USA) — with 6-MV flattening filter-free beams. Based on the RANDO phantom, virtual lung and liver phantoms were created for treatment planning (Figs. 1 and 2). The electron

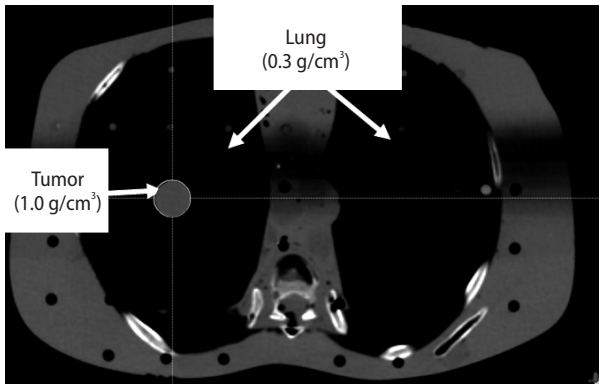

Figure 1. The locations of the target evaluated in the virtual non-homogeneous phantom. The virtual sphere target was set to the center positions of the right lung. The density of the lung and target were assigned to 0.3 g/cm^3 and 1.0 g/cm^3, respectively. The radius of the tumor was 1.0 cm

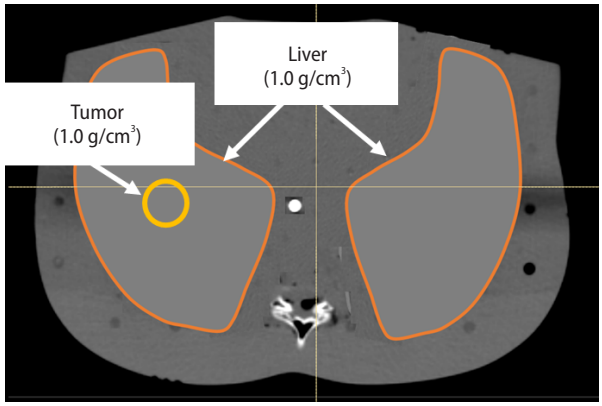

Figure 2. The locations of the target evaluated in the virtual homogeneous phantom. The virtual liver and sphere target were set to the center positions of the right liver. The density of both the liver and target was assigned to 1.0 g/cm^3. The radius of the tumor was 1.0 cm

density of the virtual sphere tumor was 1.0 g/cm^3. The radius of the virtual sphere tumor was 1.0 cm in the homogeneous and nonhomogeneous phantoms. The electron densities of the virtual lung and liver were 0.3 and 1.0 g/cm^3, respectively. The virtual tumor region was defined as the gross tumor volume (GTV) = CTV. A PTV margin was added 5–20 mm around the CTV. A volumetric modulated arc therapy (VMAT) plan was created using noncoplanar angles. The gantry angle was set counterclockwise at 0°–180°. The collimator and couch angles were fixed at 10° and 0°, respectively. A dose of 24–66 Gy was prescribed for D95% of the PTV.

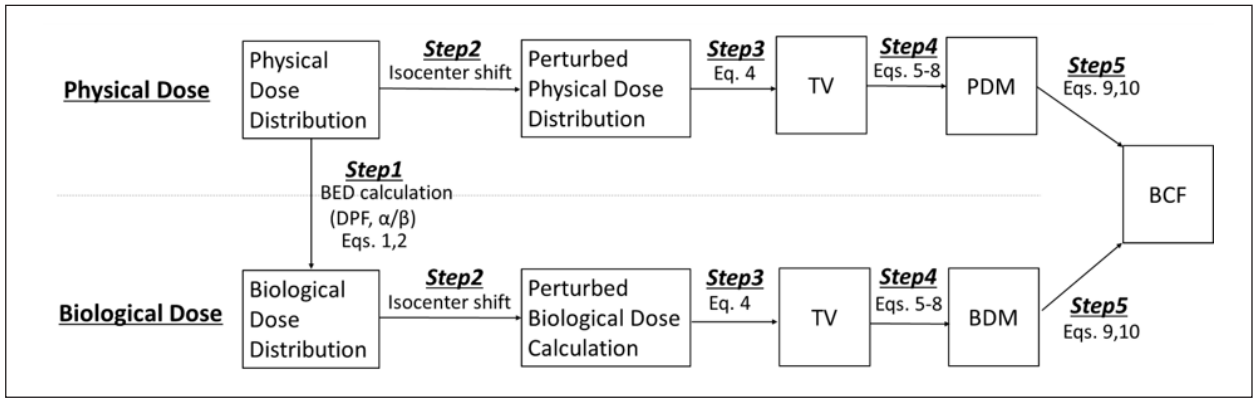

Figure 3. The process of evaluating the biological dosimetric margin (BDM) and physical DM (PDM), which referred from our previous study [4]

Figure 3 shows the scheme for calculating the BDM and PDM which were obtained from our previous study [11]. The BED was converted from the physical dose using the linear quadratic (LQ) model (Step 1).

$$BED = nd\left(1 + \frac{d}{\alpha/\beta}\right) \quad (1)$$

where n is the fractionation and d is the DPF. The LQ model fits the cell-surviving fraction through a second-order polynomial on the DPF with coefficients α/β, which shows the repair capacity of the cells. The DPF and α/βmainly affected the BDM. In this study, α/β was set to 3 Gy for the normal tissue and 10 Gy for the tumor. Dose and fraction schemes differed for each clinical trial. In the current study, the DPF was in the range of 3–20 Gy, referring to the previous study of lung SBRT [12–19] and liver SBRT [20].

The biological and physical dose distributions considering the setup uncertainty were calculated in the RayStation treatment planning system. The isocenter was shifted from –30 to 30 mm along the left–right (LR) direction (Δ_L and Δ_R), –30 to 30 mm along the anterior–posterior (AP) direction (Δ_A and Δ_P), and –30 to 30 mm along the cranio-caudal (CC) direction (Δ_{Cr} and Δ_{Ca}) (Step 2). The treated volume (TV) and DM proposed in the previous study are shown in Fig. 4. In the current study, TV is defined as the volume that satisfies

$$TV = V_{D_{95\%}^{CTV} \geq 0.9 \times D_{Rx}} \quad (2)$$

where D_X^{ROI} is the dose to the region of interest (ROI) and X is 95% of the prescribed physical and biological doses by shifting the isocenter. D_{Rx} denotes the prescribed dose. Subsequently, the maximum shifts toward the LR, AP, and CC directions (Δ_L, Δ_R, Δ_A, Δ_P, Δ_{Cr}, and Δ_{Ca}) that followed the passed criteria.

$$D_{95\%}^{CTV} \geq 0.9 \times D_{Rx} \quad (3)$$

The DM by shifting the isocenter was calculated as

$$DM_x = (\Delta_L + \Delta_R)/2 \quad (4)$$

$$DM_y = (\Delta_A + \Delta_P)/2 \quad (5)$$

$$DM_z = (\Delta_{Cr} + \Delta_{Ca})/2 \quad (6)$$

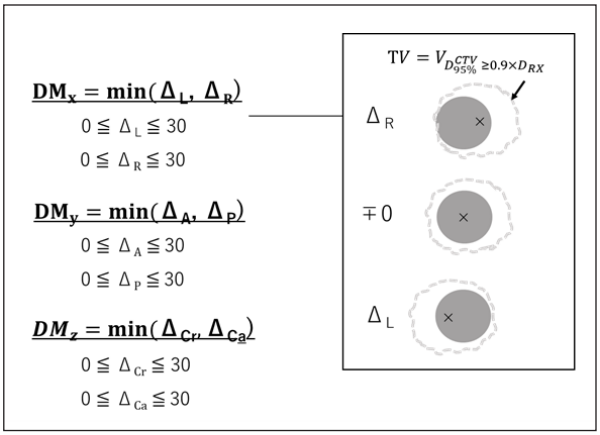

Figure 4. The dosimetric margin (DM) and the treated volume (TV) proposed in our study. See text for details. BDM — biological dosimetric margin; PDM — physical DM; BCF — biological conversion factor

The anisotropic physical DM (PDM) and biological DM (BDM) were calculated from TV and CTV (Step 3), respectively.

The BCF model was calculated as follows (Step 4):

$$BCF = \frac{BDM}{PDM} \quad (7)$$

The BCF was fitted using $d/(\alpha/\beta)$. The fitting equation was modified from that of our previous fitting model. This was because the PTV margin had a constant value in the previous study. The fitting model was expanded to fit the various sizes of the PTV margins in the homogeneous and nonhomogeneous tumor regions.

$$BCF = (A \times M + B)\, ln\left(\frac{d}{\alpha/\beta}\right) + (C \times M + D) \quad (8)$$

A, B, C, and D are the optimized fitting parameters obtained using the least squares method. M shows the PTV margin from 5 to 20 mm. The fitting equation was determined by calculating the BDM.

Results

Physical and biological DMs in a virtual nonhomogeneous phantom

Figure 5 shows the PDM and BDM at a DPF of 3–20 Gy along the LR, AP, and CC directions with an isotropic PTV margin of 5–20 mm in the nonhomogeneous phantom. The maximum difference between the directions was 0.6, 1.9, 3.1, and 5.3 mm with PTV margins of 5, 10, 15, and 20 mm, respectively. Figure 6 shows the BCF at a DPF of 3–20 Gy along the LR, AP, and CC directions. The difference in the BCF was within 0.01 with a PTV margin of 5 mm, 0.02 with a PTV margin of 10–15 mm, and 0.03 with a PTV margin of 20 mm. Figure 7A shows the average BCF along the LR, AP, and CC directions with a PTV margin of 5–20 mm. There was no significant difference in the data with a PTV margin of 10–20 mm. Thus, the BCF was fitted after combining the data with a PTV margin of 10–20 mm. Thus, M was 5 for a PTV margin of 5 mm and 10 for a PTV margin of 10–20 mm. The resulting fitting parameters of the BCF are shown in Figure 7B (the parameters are listed in Tab. 1).

Physical and biological DMs in a virtual homogeneous phantom

Figure 8 shows the PDM and BDM at a DPF of 3–20 Gy along the LR, AP, and CC directions with an isotropic PTV margin of 5–20 mm in a homogeneous phantom. The maximum difference between the directions was 1.15, 1.8, 4.5, and 5.7 mm with PTV margins of 5, 10, 15, and 20 mm, respectively. Fig. 9 shows the BCF at a DPF of 3–20 Gy along the LR, AP, and CC directions. The difference in the BCF was within 0.03 with a PTV margin of 5 mm, and 0.05 with a PTV margin of 10–20 mm. Figure 10 shows the average BCF along the LR, AP, and CC directions and the fitted BCF curve with a PTV margin of 5–20 mm. The fitting parameters for the BCF are listed in Table 2.

Discussion

The PTV margin is a geometrical concept that incorporates geometrical variations and inaccuracies [21]. Gordon proposed a DM that considers the relation between the PTV and dose distribution. In the previous study, the BED was used to compare the biological effects of the prescribed dose [4, 12–19]. Biological damage depends on the DPF. The current study evaluated the BDM and BCF, which are the conversion factors of PDM to BDM in homogeneous and nonhomogeneous tumor regions.

In the current study, the BDM was evaluated in the virtual homogeneous and nonhomogeneous phantoms. Moreover, the BCF fitting model expanded with the size of the PTV margin in the homogeneous and nonhomogeneous regions. The BDM was smaller than the PDM in the LR, AP, and CC directions for the DPFs in the homogeneous and nonhomogeneous tumor regions. In the nonhomogeneous region, the difference in the BCF with a PTV margin of 10–20 mm was smaller, and these exhibited a larger difference with the BCF with a PTV margin of 5 mm. The tumor scattering decreased with an increase in the distance from the tumor. For a PTV margin of 5 mm, the relation between the tumor and scattering changed owing to perturbation. For a PTV margin of 10–20 mm, the ratio of the tumor to the PTV was small, and it had a negligible effect on the tumor scattering in the stationary phase without perturbation.

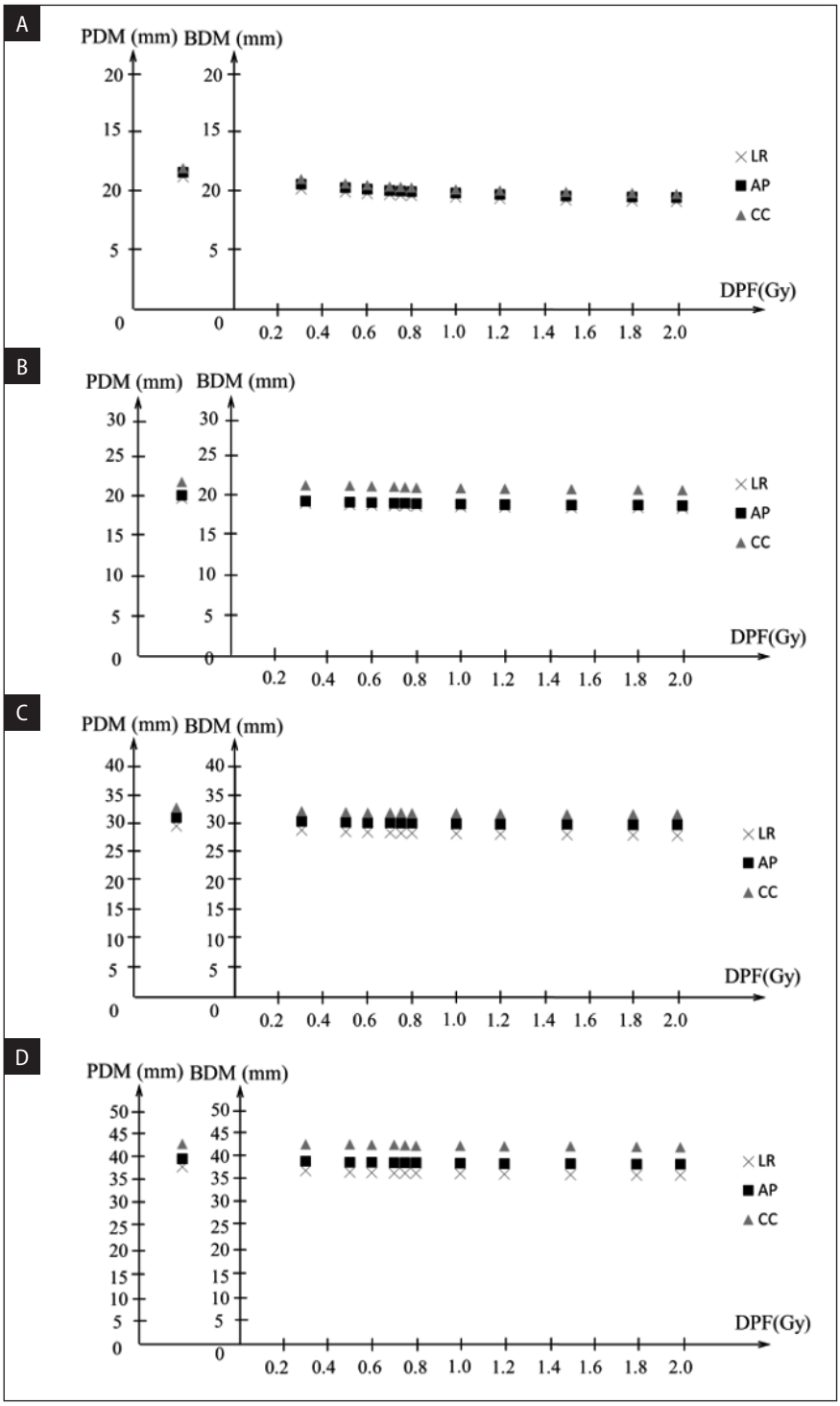

Figure 5. Measured physical dosimetric margin (PDM) and biological dosimetric margin (BDM) at the dose per fraction (DPF) of 3–20 Gy in left–right (LR), anterior–posterior (AP), and cranio-caudal (CC) directions for the margin with an isotropic planning target volume (PTV) margin of 5 mm (**A**), 10 mm (**B**), 15 mm (**C**), and 20 mm (**D**) in non-homogeneous phantom

The PDM can be calculated using the geometric PTV margin obtained through commercial treatment planning in the clinical process. Then, the optimal BDM can be derived considering the size of the PTV margin for the BED in the homogeneous and nonhomogeneous regions when the DPF is changed.

The BED calculation using the LQ model did not correspond to the repair and proliferation of the tumors. A recent study showed that the LQ model

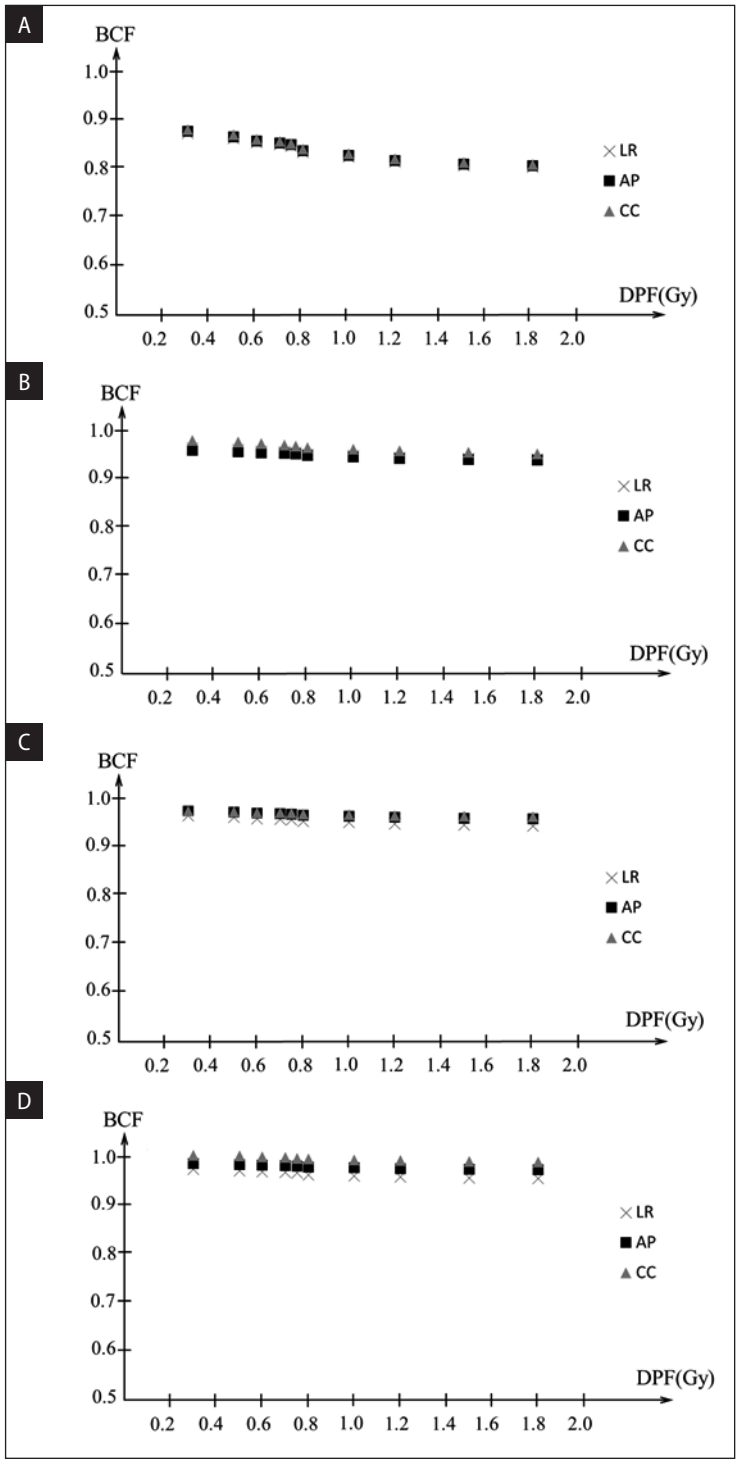

Figure 6. The calculated biological conversion factor (BCF), the average BCF in left–right (LR), anterior–posterior (AP), and cranio-caudal (CC) directions with an isotropic planning target volume (PTV) margin of 5 mm (**A**), 10 mm (**B**), 15 mm (**C**), and 20 mm (**D**) in a non-homogeneous phantom

underestimates tumor control performed by SBRT and stereotactic radiosurgery (SRS) because it does not consider indirect cell death [22–24]. Our study incorporated the BED into the margin. This BED model can be applied to other tumor types and biological models [25, 26] using the proposed procedure.

The radiobiological model has been improved to fit hypofractionation or other radiotherapy irradiation techniques. In the future, the BED should

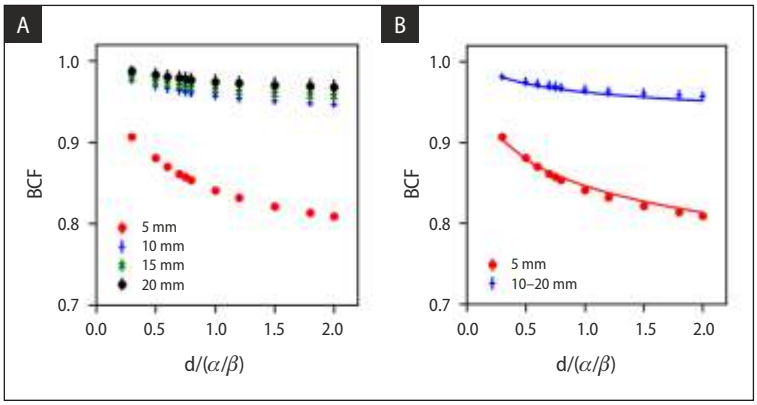

Figure 7. A. The calculated biological conversion factor (BCF), the average BCF in left–right (LR), anterior–posterior (AP), and cranio-caudal (CC) directions with a planning target volume (PTV) margin of 5–20 mm for a non-homogeneous phantom. Closed red circles, blue plus symbols, green cross symbols, closed black circles are the data of the BCF with PTV margin of 5 mm, 10 mm, 15 mm, and 20 mm, respectively. Error bars represent the standard error of the mean in LR, AP, and CC directions; **B.** The fitted BCF curve with a PTV margin of 5 mm (closed red circle and red line) and 10–20 mm (blue plus symbols and blue line). The parameter M is 5 used for the PTV margin of 5 mm and 10 for the PTV margin of 10–20 mm

Table 1. The fitting parameters using Eq. (8) in virtual non-homogeneous phantom

Parameter	Value	SD
A	–4.1e–03	2.1e–04
B	–3.5e–03	1.1e–04
C	2.5e–03	1.6e–03
D	8.0e–02	1.0e–03

SD — standard deviation

be used to compare different dose fractionation schemes and improve the margin model by evaluating the BED distribution.

Conclusion

The current study helped improve the estimation of the BDM based on the physical dose distribution and size of the PTV margin. Moreover, the improved BCF model can be useful to calculate the BED coverage of the target tumor volume in homogeneous and nonhomogeneous regions.

Conflict of interest

None declared.

Funding

None declared.

References

1. Dale RG, Dale RG. The application of the linear-quadratic dose-effect equation to fractionated and protracted radiotherapy. Br J Radiol. 1985; 58(690): 515–528, doi: 10.1259/0007-1285-58-690-515, indexed in Pubmed: 4063711.
2. Jones B, Dale RG, Deehan C, et al. The role of biologically effective dose (BED) in clinical oncology. Clin Oncol (R Coll Radiol). 2001; 13(2): 71–81, doi: 10.1053/clon.2001.9221, indexed in Pubmed: 11373882.
3. Aparicio DZ, Requejo OH, de Julián MÁ, et al. Local control rates in stereotactic body radiotherapy (SBRT) of lung metastases associated with the biologically effective dose. Rep Pract Oncol Radiother. 2019; 24(2): 142–150, doi: 10.1016/j.rpor.2019.01.001, indexed in Pubmed: 30723385.
4. Fowler JF, Rezvani M, Fowler JF, et al. The first James Kirk memorial lecture. What next in fractionated radiotherapy? Br J Cancer Suppl. 1984; 6(2): 285–300, indexed in Pubmed: 6365141.
5. Aparicio DZ, Requejo OH, de Julián MÁ, et al. Local control rates in stereotactic body radiotherapy (SBRT) of lung metastases associated with the biologically effective dose. Rep Pract Oncol Radiother. 2019; 24(2): 142–150, doi: 10.1016/j.rpor.2019.01.001, indexed in Pubmed: 30723385.
6. Ekstrand KE, Barnes WH. Pitfalls in the use of high energy X rays to treat tumors in the lung. Int J Radiat Oncol Biol Phys. 1990; 18(1): 249–252, doi: 10.1016/0360-3016(90)90290-z, indexed in Pubmed: 2105286.
7. Klein EE, Morrison A, Purdy JA, et al. A volumetric study of measurements and calculations of lung density corrections for 6 and 18 MV photons. Int J Radiat Oncol Biol Phys. 1997; 37(5): 1163–1170, doi: 10.1016/s0360-3016(97)00110-7, indexed in Pubmed: 9169827.

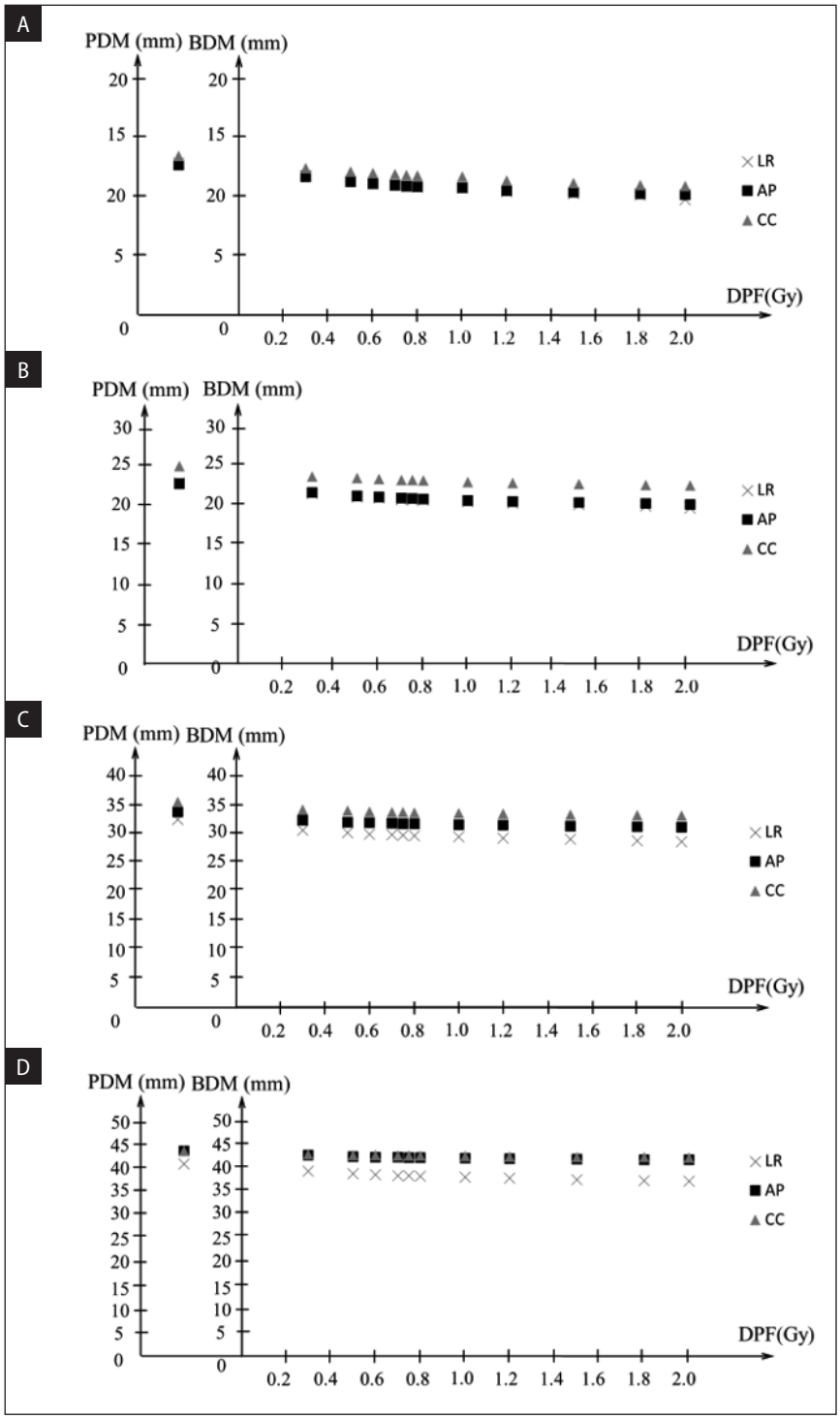

Figure 8. Measured physical dosimetric margin (PDM) and biological dosimetric margin (BDM) at the dose per fraction (DPF) of 3–20 Gy in left–right (LR), anterior–posterior (AP), and cranio-caudal (CC) directions for the margin with an isotropic planning target volume (PTV) margin of 5 mm (**A**), 10 mm (**B**), 15 mm (**C**), and 20 mm (**D**) in a homogeneous phantom

8. Knöös T, Ahnesjö A, Nilsson P, et al. Limitations of a pencil beam approach to photon dose calculations in lung tissue. Phys Med Biol. 1995; 40(9): 1411–1420, doi: 10.1088/0031-9155/40/9/002, indexed in Pubmed: 8532755.
9. Jiang SB, Pope C, Al Jarrah KM, et al. An experimental investigation on intra-fractional organ motion effects in lung IMRT treatments. Phys Med Biol. 2003; 48(12): 1773–1784, doi: 10.1088/0031-9155/48/12/307, indexed in Pubmed: 12870582.
10. Adamczyk M, Kruszyna-Mochalska M, Rucińska A, et al. Software simulation of tumour motion dose effects during flattened and unflattened ITV-based VMAT

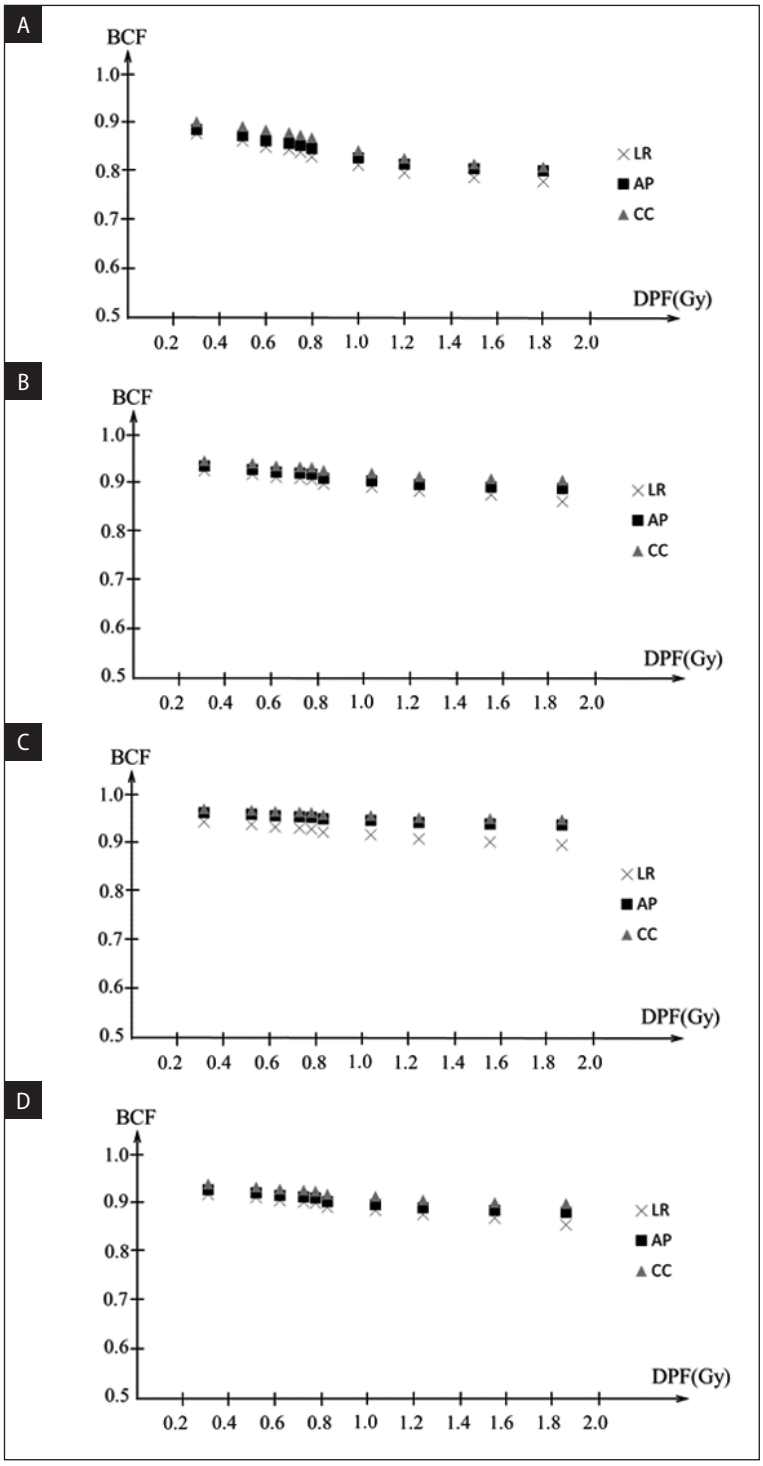

Figure 9. The calculated biological conversion factor (BCF) the average BCF in left–right (LR), anterior–posterior (AP), and cranio-caudal (CC) directions with an isotropic planning target volume (PTV) margin of (**A**) 5 mm, (**B**) 10 mm, (**C**) 15 mm, and (**D**) 20 mm in a homogeneous phantom

lung SBRT. Rep Pract Oncol Radiother. 2020; 25(4): 684–691, doi: 10.1016/j.rpor.2020.06.003, indexed in Pubmed: 32581656.
11. Kawahara D, Saito A, Ozawa S, et al. Consequently, the dose perturbation affects the BDM distribution and BCF model. . J Appl Clin Med Phys. 2020; 21(4): 31–41.
12. Shen GE, Wanf YJ, Shen WJ, et al. Stereotactic body radiation therapy for centrally-located lung tumors. Oncol Lett. 2014; 7(4): 1292–1296, doi: 10.3892/ol.2014.1815, indexed in Pubmed: 24944711.
13. Onimaru R, Shirato H, Shimizu S, et al. Tolerance of organs at risk in small-volume, hypofractionated, im-

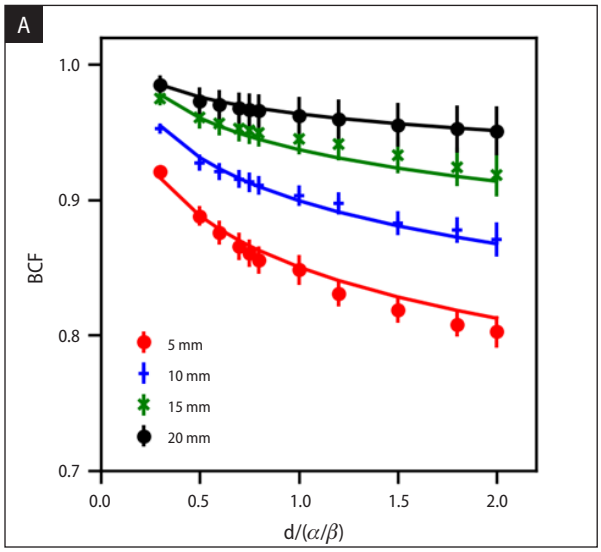

Figure 10. The calculated biological conversion factor (BCF) plot and fitted BCF curve with planning target volume (PTV) margin of 5 mm (closed red circle and red line), 10 mm (blue plus symbols and blue line), 15 mm (green plus cross and green line), 20 mm (black circle symbols and black line)

Table 2. The fitting parameters using Eq. (8) in virtual homogeneous phantom

Parameter	Value	SD
A	8.7e–03	8.1e–04
B	–1.3e–02	1.1e–03
C	–0.1	1.0e–02
D	2.8e–03	1.3e–04

SD — standard deviation

age-guided radiotherapy for primary and metastatic lung cancers. Int J Radiat Oncol Biol Phys. 2003; 56(1): 126–135, doi: 10.1016/s0360-3016(03)00095-6, indexed in Pubmed: 12694831.
14. Uematsu M, Shioda A, Suda A, et al. Computed tomography-guided frameless stereotactic radiotherapy for stage I non-small cell lung cancer: a 5-year experience. Int J Radiat Oncol Biol Phys. 2001; 51(3): 666–670, doi: 10.1016/s0360-3016(01)01703-5, indexed in Pubmed: 11597807.
15. Nagata Y, Takayama K, Matsuo Y, et al. Clinical outcomes of a phase I/II study of 48 Gy of stereotactic body radiotherapy in 4 fractions for primary lung cancer using a stereotactic body frame. Int J Radiat Oncol Biol Phys. 2005; 63(5): 1427–1431, doi: 10.1016/j.ijrobp.2005.05.034, indexed in Pubmed: 16169670.
16. Taremi M, Hope A, Dahele M, et al. Stereotactic body radiotherapy for medically inoperable lung cancer: prospective, single-center study of 108 consecutive patients. Int J Radiat Oncol Biol Phys. 2012; 82(2): 967–973, doi: 10.1016/j.ijrobp.2010.12.039, indexed in Pubmed: 21377293.
17. Wulf J, Haedinger U, Oppitz U, et al. Stereotactic radiotherapy for primary lung cancer and pulmonary metastases: a noninvasive treatment approach in medically inoperable patients. Int J Radiat Oncol Biol Phys. 2004; 60(1): 186–196, doi: 10.1016/j.ijrobp.2004.02.060, indexed in Pubmed: 15337555.
18. Olsen JR, Robinson CG, El Naqa I, et al. Dose-response for stereotactic body radiotherapy in early-stage non-small-cell lung cancer. Int J Radiat Oncol Biol Phys. 2011; 81(4): e299–e303, doi: 10.1016/j.ijrobp.2011.01.038, indexed in Pubmed: 21477948.
19. Timmerman R, Papiez L, McGarry R, et al. Extracranial Stereotactic Radioablation: results of a phase I study in medically inoperable stage I non-small cell lung cancer. Chest. 2003; 124(5): 1946–1955, doi: 10.1378/chest.124.5.1946, indexed in Pubmed: 14605072.
20. Robbins JR, Schmid RK, Hammad AY, et al. Stereotactic body radiation therapy for hepatocellular carcinoma: Practice patterns, dose selection and factors impacting survival. Cancer Med. 2019; 8(3): 928–938, doi: 10.1002/cam4.1948, indexed in Pubmed: 30701703.
21. van Herk M, Remeijer P, Rasch C, et al. The probability of correct target dosage: dose-population histograms for deriving treatment margins in radiotherapy. Int J Radiat Oncol Biol Phys. 2000; 47(4): 1121–1135, doi: 10.1016/s0360-3016(00)00518-6, indexed in Pubmed: 10863086.
22. Kawahara D, Wu L, Watanabe Y. Optimization of irradiation interval for fractionated stereotactic radiosurgery by a cellular automata model with reoxygenation effects. Phys Med Biol. 2020; 65(8): 085008, doi: 10.1088/1361-6560/ab7974, indexed in Pubmed: 32092715.
23. Kawahara D, Nagata Y, Watanabe Y. Improved cellular automata model shows that indirect apoptotic cell death due to vascular damage enhances the local control of tumors by single fraction high-dose irradiation. Biomed Phys Eng Express. 2021; 8(1), doi: 10.1088/2057-1976/ac4466, indexed in Pubmed: 34920444.
24. Brown JM, Carlson DJ, Brenner DJ. The tumor radiobiology of SRS and SBRT: are more than the 5 Rs involved? Int J Radiat Oncol Biol Phys. 2014; 88(2): 254–262, doi: 10.1016/j.ijrobp.2013.07.022, indexed in Pubmed: 24411596.
25. Guerrero M, Li XA. Extending the linear-quadratic model for large fraction doses pertinent to stereotactic radiotherapy. Phys Med Biol. 2004; 49(20): 4825–4835, doi: 10.1088/0031-9155/49/20/012, indexed in Pubmed: 15566178.
26. Astrahan M. Some implications of linear-quadratic-linear radiation dose-response with regard to hypofractionation. Med Phys. 2008; 35(9): 4161–4172, doi: 10.1118/1.2969065, indexed in Pubmed: 18841869.